Improved seismic fragility analysis method using BOX-COX regression and Monte Carlo Sampling technique

Penghui Zhang, Zhiqiang Wang & Wancheng Yuan
Tongji University, Shanghai, China

ABSTRACT: The cloud method is one of the main tools for calculating the analytical fragility curves. However, the assumptions of this method, viz., linearity, normality and homoscedasticity, which are aimed at simplifying the calculation process, are usually not consistent with the actual results. To solve this problem, a new fragility analysis method is proposed by combining BOX-COX regression and Monte Carlo Sampling technique. This method does not increase the times of the nonlinear time history analysis, and also need not restrict to the three basic assumptions of the cloud method. A three-span concrete continuous girder bridge is taken as an example to verify the validity of the method developed. Subsequently, the results obtained from the proposed method are compared with those of cloud method employing the determination coefficient (R^2), Kernel Density Estimation curve, and the rank-correlation coefficient. The result indicates that BOX-COX regression can improve the linearity, normality and homoskedasticity of the probabilistic seismic demand model (PSDM), ensuring the accuracy of fragility analysis. The fragility curves derived applying cloud method will lead to errors when the basic assumptions are not satisfied, and the errors increase with the damage state increasing.

1 INTRODUCTION

The analytical fragility curve is one of the most popular tools to assess the potential seismic risk of bridge structures (Muntasir Billah and Shahria Alam, 2015). Based on the fragility analysis, the relationship between the ground motion intensity measure (IM) and the probability that the structural demand exceeds a given limit state (LS) is established. Owing to its computational efficiency, the cloud method has become one of the fundamental approaches to establish the analytical fragility curve (Nielson and DesRoches, 2007a). Nevertheless, the assumptions of this method, that is, normality, linearity and homoscedasticity aiming at simplifying the analysis process, are normally inconsistent with the actual outcomes (Baker, 2007, Karamlou and Bocchini, 2014). This can be interpreted further as: (a) the engineering demand parameter (EDP) under a given IM does not strictly follow the lognormal distribution; (b) poor linear correlation between $\ln(\mathrm{IM})$ and $\ln(\mathrm{EDP})$ exists in some cases, where $\ln(\bullet)$ is the natural logarithm function; (c) the variance of $\ln(\mathrm{EDP})$ varies with the change of IM.

Considerable studies have focused on these three problems existed in the cloud method. Karamlou and Bocchini (2014) studied the influence of these three assumptions on analytical fragility curve by a large number of numerical analyses considering the uncertainties of structural material and modeling parameters. Results implied that problem (a) does not lead to a significant error on the fragility curve while the others do. In terms of the problem (b), most studies concentrated on developing or selecting an optimal IM which has a significant logarithmic linear relation with the EDP for specific site conditions and structure types. The vector-based IM (Baker, 2007), fractional order IM (Shafieezadeh et al., 2012), posteriori optimal IM (Du et al., 2019) and many other IMs were proposed. On the other hand, some researchers considered the nonlinear relationship between $\ln(\mathrm{IM})$ and $\ln(\mathrm{EDP})$, and established PSDMs with quadratic regression (Pan et al., 2007) and bilinear regression (Mackie and Stojadinović, 2005). In order to avoid the problems of cloud method, researchers have used other methods to obtain the analytical fragility curve, such as incremental dynamic analysis (IDA) (Vamvatsikos and Cornell, 2001) and Bayesian approach (Gardoni et al., 2002). However, the application of IDA is limited because of the increase in the number of time history analysis and the scaling of ground motions (Mackie and Stojadinovic, 2002). Meanwhile, the Bayesian approach faces the challenge of computational complexity, and can only be applied to simple structures at present (Zhong et al., 2008, Huang et

al., 2010). Therefore, it is essential to put forward a fragility analysis method which can be free from the aforementioned three basic assumptions without increasing the times of time history analysis.

This paper aims at improving the reliance of fragility analysis without a significant increase in the computational cost. Firstly, the basic processes of cloud method and BOX-COX regression were introduced briefly to show the advantages of the Box-Cox regression model in handling nonlinear, non-normality and heteroskedasticity problems by data transforming. Then, a new fragility analysis method was proposed by combining BOX-COX regression and Monte Carlo Sampling (MCS) technique. Finally, a three-span concrete continuous girder bridge was taken as an example to verify the effectiveness of this method.

2 BOX-COX REGRESSION

The least squares linear (LSL) regression model was adopted to predict the values of the response variable using the independence variable when these two variables meet the significant linear correlation, as expressed in Eq. (1):

$$y = \alpha_0 + \alpha_1 x + e \tag{1}$$

Where α_0 and α_1 are regression coefficients; x and y are the independence and response variable, respectively; and e is the residual error.

The least squares linear regression contains four basic assumptions, namely, (a) significant linear correlation between variables x and y; (b) residual error e follows the normal distribution; (c) the variance of residual error is constant; and (d) the residual error is mutually independent. Because of the using of LSL regression, the four aforementioned basic assumptions should be followed in the cloud method, but the first three assumptions are often not consistent with the actual outcomes of the probabilistic seismic demand model (PSDM).

The Box-Cox regression model was proposed to handle nonlinearity, non-normality and heteroskedasticity of linear regression by data transformation (Collins, 1991). The BOX-COX transformation was proposed by Box and Cox in 1964, written as Eq. (2) (Box and Cox, 1964).

$$y^{(\lambda)} = \begin{cases} \dfrac{(y+s)^{\lambda}-1}{\lambda}, & \lambda \neq 0 \\ \ln(y+s), & \lambda = 0 \end{cases} \tag{2}$$

Where s is a coefficient used to make the algebraic sum of y and s greater than 0. If $y > 0$, $s = 0$. Otherwise, $s = \text{ceil}(|\min(y)|)$, ceil(•) is the up-round function. Applying the BOX-COX transformation to the response variable in Eq. (1) leads to the Box-Cox regression model, written as Eq. (3).

$$y^{(\lambda)} = \alpha_0' + \alpha_1' x + e' \tag{3}$$

The optimal value of λ is determined by the maximum likelihood estimation method. Assuming e_i' is a random variable obeying the normal distribution with zero mean and variance σ'^2, the joint probability density function of residual error vector $\mathbf{e}' = (e_1', e_2', ..., e_n')$ takes the form as Eq. (4).

$$f(\mathbf{e}') = (2\pi\sigma'^2)^{-\frac{n}{2}} \exp\left\{-\frac{1}{2\sigma'^2}\sum_{i=1}^{n} e_i'^2\right\} \tag{4}$$

Then, the joint probability density function of the response vector $\mathbf{y} = (y_1, y_2, ..., y_n)$ can be written as Eq. (5).

$$f(\mathbf{y}) = (2\pi\sigma'^2)^{-\frac{n}{2}} \exp\left\{-\sum_{i=1}^{n}\frac{[y_i^{(\lambda)} - (\alpha_0' + \alpha_1' x_i)]^2}{2\sigma'^2}\right\}\prod_{i=1}^{n} y_i^{\lambda-1} \tag{5}$$

Taking natural logarithm at Eq. (6) yielding the likelihood function:

$$L(\lambda) = (\lambda-1)\sum_{i=1}^{n}\ln(y_i) - \frac{n}{2}\ln\left\{\sum_{i=1}^{n}\frac{[y_i^{(\lambda)} - (\alpha_0' + \alpha_1' x_i)]^2}{n-2}\right\} \tag{6}$$

It is difficult to obtain partial derivatives for Eq. (6), therefore the optimal numerical solution value of the coefficient λ, which maximizes $L(\lambda)$, is searched with searching step size 0.01.

3 THE CLOUD METHOD

Cornell et al. (2002) found that the relationship between the mean value of EDP (S_D) and IM can be estimated using a power model:

$$S_D = a\text{IM}^b \tag{7}$$

This can be rewritten to perform a LSL regression model as the following form:

$$\ln(\text{EDP}) = a + b\ln(\text{IM}) + e, \quad e \sim N(0, \beta_D^2) \tag{8}$$

Where a and b are regression coefficients obtained using ordinary least squares method. Due to the adoption of least squares linear regression, the assumptions of normality, linearity and homoscedasticity should be followed when the cloud method is used. The conditional probability that a bridge component (i.e. abutments, bearings, columns) experiences a certain level of demand (D) at a given IM level can be shown as Eq. (9):

$$P[D > d \mid \text{IM}] = 1 - \Phi\left[\frac{\ln(d) - \ln(S_D)}{\beta_D}\right] \tag{9}$$

Where the logarithmic standard deviation of seismic demand is valued as Eq. (10).

$$\beta_D = \sqrt{\frac{\sum_{i=1}^{n}[\ln(D_i) - a - b\ln(\mathrm{IM}_i)]^2}{n-2}} \quad (10)$$

When the capacity (C) is also assumed to follow a lognormal distribution, the bridge component fragility at j-th limit state (LS_j) takes the form of Eq. (11).

$$P[LS_j \mid \mathrm{IM}] = \Phi\left[\frac{\ln(S_D) - \ln(S_C)}{\sqrt{\beta_D^2 + \beta_C^2}}\right] \quad (11)$$

Where S_C and β_C are the mean and logarithmic standard deviation of structural capacity on LS_j.

4 THE IMPROVED SEISMIC FRAGILITY ANALYSIS METHOD

To eliminate the influence of the three basic assumptions adopted in cloud method without significant increase of the computational cost, a new fragility analysis method is proposed by combining BOX-COX regression and Monte Carlo Sampling (MCS) technique. Firstly, BOX-COX regression is adopted to generate the PSDM. Equation (8) is updated to Equation (12):

$$\ln(\mathrm{EDP})^{(\lambda)} = a' + b'\ln(\mathrm{IM}) + e', \quad e' \sim N(0, \beta_D'^2) \quad (12)$$

Where a' and b' are regression coefficients obtained using ordinary least squares method. In the improved method, the $\ln(\mathrm{EDP})^{(\lambda)}$, instead of $\ln(\mathrm{EDP})$, is a normally distributed random variable with mean $a' + b'\ln(\mathrm{IM})$ and variance $\beta_D'^2$, thereby the component fragility can no longer be written in the simple form of Eq. (11). A number of $\ln(D)^{(\lambda)}$ are then generated using the MCS technique. The times of sampling is usually taken as 10^6 (Nielson and DesRoches, 2007b). $\ln(D)$ is adopted using BOX-COX inverse transformation shown as Eq. (13).

$$\ln(D) = \begin{cases} \left[\lambda\ln(D)^{(\lambda)} + 1\right]^{\frac{1}{\lambda}} - s, & \lambda \neq 0 \\ \exp\left[\ln(D)^{(\lambda)}\right] - \mathrm{s}, & \lambda = 0 \end{cases} \quad (13)$$

Meanwhile, a number of $\ln(C)$ with respect to LS_j, which are assumed to follow a normal distribution, are obtained using the MCS technique with sampling times of 10^6. The indicator function is used to judge each demand-capacity sample, defined as Eq. (14).

$$I_k = \begin{cases} 0, & \ln(D) < \ln(C) \\ 1, & \ln(D) \geq \ln(C) \end{cases} \quad (14)$$

Finally, the failure probability of the component takes the form as Eq. (15).

$$P[LS_j \mid \mathrm{IM}] = \frac{\sum_{k=1}^{10^6} I_k}{10^6} \quad (15)$$

5 APPLICATION EXAMPLE: A HIGHWAY BRIDGE

5.1 *Description of structure and numerical modeling*

A typical concrete continuous girder bridge with three spans of (60 m + 100 m+ 60 m) was selected as the case project. The superstructure consists of a single-cell box girder with a width of 16.3 m and the girder depth varies from 3 to 6.67 m. All of the RC piers possess the identical rectangular cross-section with sizes of 6.5 × 3.5 m, and the height of the bridge column is 9 m. For the RC piers, the concrete compression strength and the reinforcement yield strength are 26.8 MPa and 400 MPa, respectively. The reinforcement ratio and the volume-stirrup ratio are 0.8% and 1%, respectively. Spherical steel bearings placed at the pier–top are used to support the girder.

As shown in Figure 1, a detailed three-dimensional finite element model of the bridge was generated in OpenSees platform. The constitutive models for concrete, steel, pounding element, and foundations are also illustrated in Figure 1. Since the deck usually retain elastic under earthquakes, it was simulated using elastic beam-column elements with mass lumped on deck nodes. Piers were simulated using displacement-based beam-column elements with the fiber section that is comprised of the reinforcement bar, cover concrete and core concrete. The stress-strain relationship of rebar was modeled using Steel 01 material, and the nonlinear behavior of cover and core concrete was simulated by Concrete 01 material (Scott et al., 1989). The spherical steel bearings, foundations, abutments and pounding effect were modeled by zero-length elements. The yield force (F_y) of the bearing was calculated using the equation of $F_y = \mu N$, where μ is the friction coefficient (set to 0.02 (Zhou et al., 2019)), and N is the reaction force of the bearing under gravity load (Feng et al., 2018). The pile foundations were represented by three translational and three rotational springs. The simplified model was adopted to simulate abutment behavior taking accuracy and efficiency into account (Aviram et al., 2008). The passive stiffness is provided by soil and piles while the active stiffness is provided only by piles. More detailed introduction of simplified abutment model can be found in the reference (Nielson, 2005). The pounding effect was simulated with the nonlinear model proposed by Muthukumar (2003). Moreover, uncertainties come from material and geometry were considered in the finite element model.

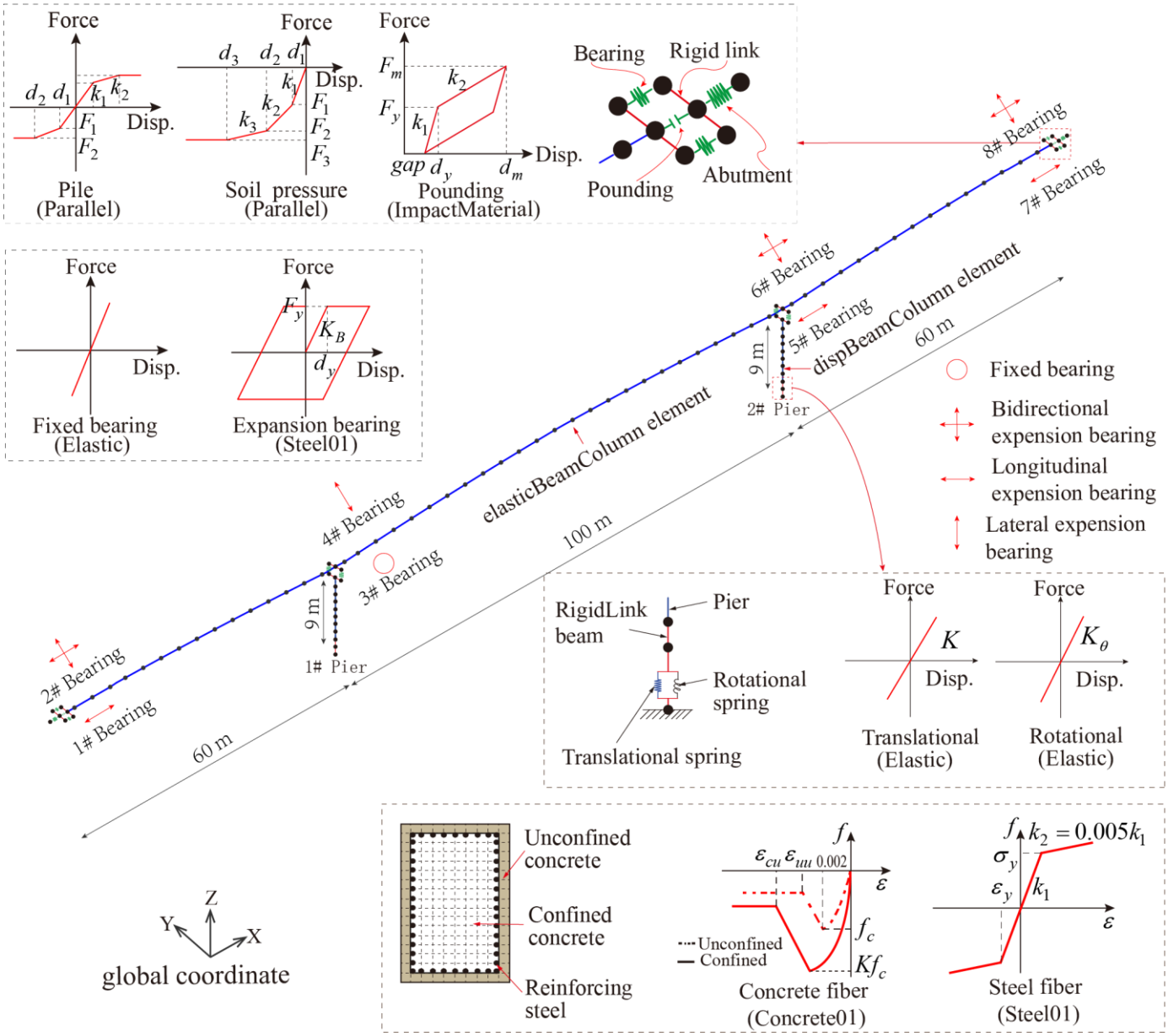

Figure 1. Numerical model of the prototype bridge

5.2 *Ground motions*

The accuracy and reliability of fragility curves greatly depend on the ground motions used for nonlinear time history analyses. The algorithm proposed by Baker and Lee (2018) can select a set of ground motions from a database while meeting the probability distribution of logarithmic spectral acceleration values generated by the ground motion prediction model (GMPM). On the basis of the site conditions, the site average shear wave velocity in the top 30 m (V_{30}) is assumed to be 205 m/s, then the median and the logarithmic standard deviation of the log-space response spectra was predicted for a magnitude 7 earthquake at a distance of 10 km (Boore et al., 2013). 100 ground motion components were selected from the NGA-West2 database (Ancheta et al., 2014) through the aforementioned algorithm with the following selection criteria: (a) moment magnitude (M) ranging from 6 to 8; (b) the closest distance to surface projection of the fault rupture (R_{jb}) less than 80 km; (c) V_{30} varying from 150 to 260 m/s. Figure 2 shows the 5% damping acceleration response spectra for each ground motion together with the mean spectra and 95% confidence interval. Statistics of magnitude and the closest distance is illustrated in Figure 3. In this study, the seismic input direction for bridge model is only limited in longitudinal direction.

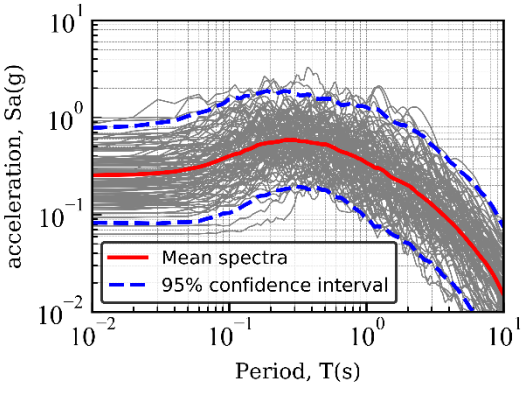

Figure 2. Acceleration response spectra (5% damping)

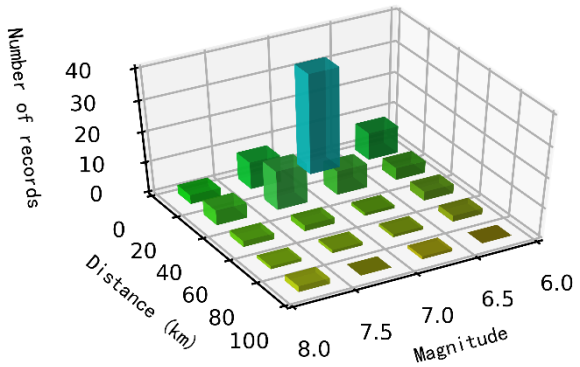

Figure 3. Statistics of magnitude and the closest distance

5.3 *probabilistic seismic demand analysis*

To establish a probabilistic seismic demand model (PSDM), the engineering demand parameter (EDP) and the ground motion intensity measure (IM) should be selected firstly. Earthquake-induced damages in abutments, bearings and columns of continuous bridges have been observed in the past earthquakes (Priestley et al., 1996). In this regard, passive abutment displacement (δ_p), active abutment displacement (δ_a), expansion bearing displacement (δ_b) and drift ratio of the fixed pier (D_r) are selected as EDPs. Moreover, the peak ground acceleration (PGA) is considered as the IM to decrease the dispersion of PSDM. PSDMs for four EDPs are developed based on least squares linear (LSL) regression and BOX-COX regression, respectively. To evaluate the normality of the residual error e, the histogram of the frequency distribution of e is plotted, meanwhile, the kernel density estimation (KDE) curve (Parzen, 1962) and the fitting normal distribution curve is obtained. The normality assumption requires consistency between the two curves. The determination coefficient (R^2), which is the square of the linear correlation coefficient of x and y, is adopted to quantitatively evaluate the linearity of the regression model. The rank correlation coefficient method is used to identify heteroscedasticity (Spearman, 1904). Sorting x and $|e|$, respectively, is required when calculating (r_s), then:

$$r_s = 1 - \frac{6}{n(n^2-1)} \sum_{i=1}^{n} d_i^2 \tag{16}$$

where d_i is the ranked difference between x_i and $|e_i|$. The p-value (p) is obtained by the significance test of r_s, and heteroskedasticity is tested with a significance level of 0.05 (Zar, 1972).

The parameters of LSL regression and BOX-COX regression are listed in Table 1. It can be reported that significant heteroscedasticity exist in LSL regression models with a significance level of 0.05 when δ_p and δ_a are adopted as EDPs. And the heteroscedasticity is eliminated when BOX-COX regression is adopted. For δ_p and δ_a, the R^2 of BOX-COX regression increase by 8.47% and 1.88%, respectively, compared with LSL regression. It implies that the linearity of the BOX-COX regression model increases while there is a nonlinear correlation between the independent variable and the response variable. It is worth noting that three basic assumptions of the cloud method are satisfied when D_r is adopted as the EDP.

Table 1. Results of LSL regression and BOX-COX regression

EDP	LSL regression			BOX-COX regression				
	R^2	r_s	p	s	λ	R^2	r_s	p
δ_p (m)	0.661	0.481	0.00	6	0.19	0.717	0.187	0.07
δ_a (m)	0.639	0.254	0.01	7	-0.29	0.651	0.153	0.13
δ_b (m)	0.543	0.184	0.07	4	0.58	0.544	0.044	0.67
D_r (%)	0.574	0.017	0.86	8	0.99	0.574	0.018	0.86

In order to show the heteroscedasticity and non-normality of residuals directly, residual graphs of LSL regression and BOX-COX regression are plotted as shown in Figure 4. Meanwhile, the Kernel Density Estimation (KDE) curve and the fitting normal distribution (Norm) curve is obtained. It can be shown that the variance of LSL regression residuals is increasing gradually with the increasing of the PGA when δ_p is selected as EDP. However, in the case of the variance, which is treated as a constant in LSL regression, the variance is overestimated in small-valued PGA range, and underestimated in large-valued PGA range. For BOX-COX regression, the variance of residuals can be considered as a constant, and residuals perform stable normality.

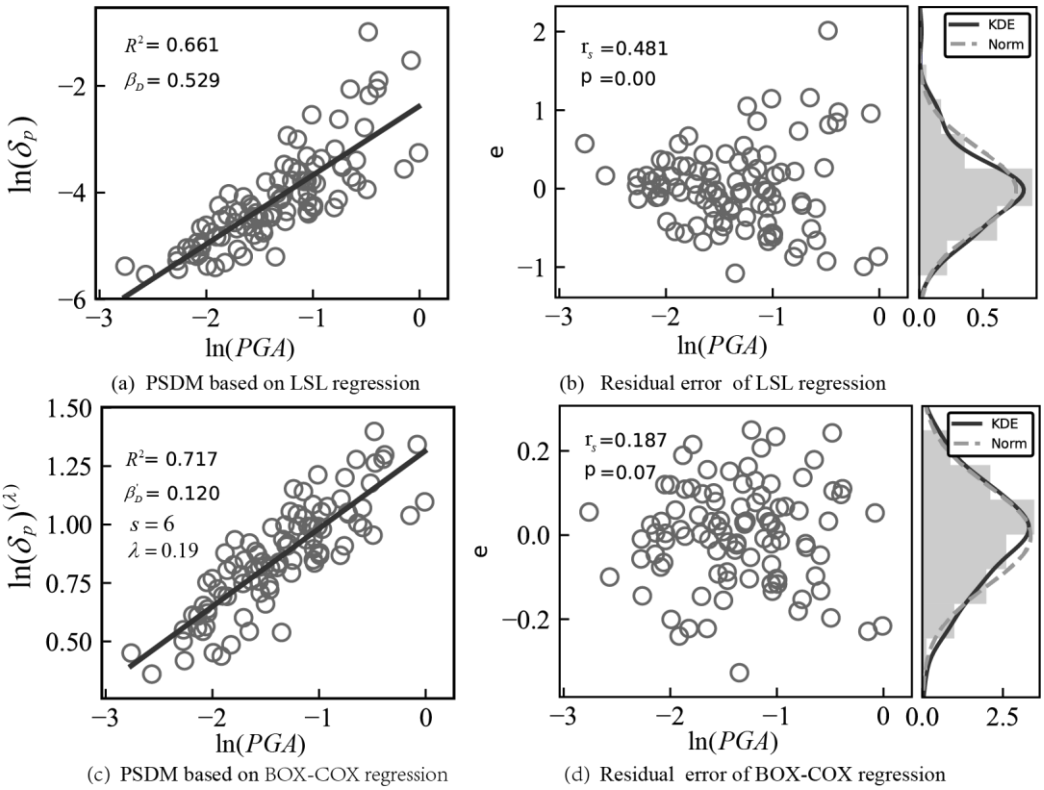

Figure 4. Comparison of LSL regression and BOX-COX regression based on δ_p

5.4 *Comparisons of fragility curves*

Defining damage states is a crucial step for establishing fragility curves. Hwang et al. (2001) suggested that bridge damage can be described as the following four damage states: slight, moderate, extensive, and complete damage. As mentioned in Section 3, each capacity limit state associated with the damage state is assumed to follow a two-parameter lognormal distribution. The median (S_C) and dispersion (β_C) for each limit state are defined for various bridge components by referring to previous research, which are summarized in Table 2.

In Figure 5, the component fragility curves for each limit state are developed based on the cloud method and the improved method, respectively. As can be seen from Figure 5(c), due to the variance overestimate in small-valued PGA range, the failure probability calculated using the cloud method is larger than that calculated using the improved method. And the failure probability calculated using the cloud method is smaller than that calculated employing the improved method because of the variance underestimation in large-valued PGA range. When heteroscedasticity and nonlinearity exist simultaneously, the deviation of failure probability calculated using the cloud method is more complicated, as shown in Figure 5(a) and 5(b). In general, the deviation exhibited by fragility curve is more obvious with increasing levels of LSs. When PGA=1g, the failure probability of δ_p for LS_2, δ_a for LS_3, and δ_b for LS_2 calculated using the cloud method is underestimated by 193.4%, 5.3%, and 35.3%, respectively. Therefore, fragility curves are unreliable if the cloud method is still adopted. Note that when all assumptions regarding the cloud method are satisfied, fragility curves developed by the cloud method is the same as those obtained by the improved method, as can be seen in Figure 5(d).

Table 2. Means and dispersions for component LS_j

EDP	LS_1 (slight)		LS_2 (moderate)		LS_3 (extensive)		LS_4 (complete)		Reference
	S_C	β_C	S_C	β_C	S_C	β_C	S_C	β_C	
δ_p (m)	37.0	0.46	146	0.46	-	-	-	-	Nielson and DesRoches (2007a)
δ_a (m)	9.8	0.70	37.9	0.90	77.2	0.85	-	-	Nielson and DesRoches (2007a)
δ_b (m)	0.15	0.35	0.35	0.35	-	-	-	-	Feng et al. (2018)
D_r (%)	0.5	0.25	1.0	0.25	2.0	0.46	2.5	0.46	Jeon et al. (2015)

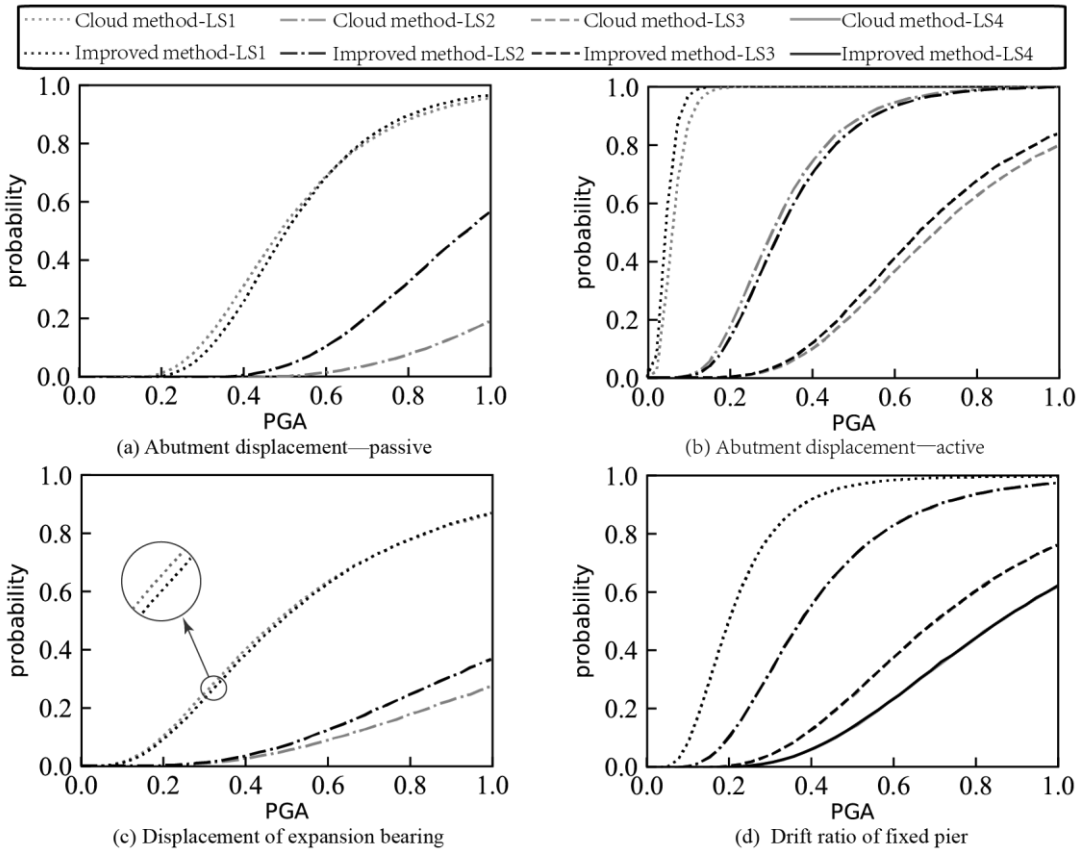

Figure 5. Component fragility curves

6 CONCLUSIONS

An improved fragility analysis method is proposed to eliminate the errors caused by assumptions of linearity, normality and homoscedasticity adopted in the cloud method. Based on a three-span concrete continuous girder bridge, a numerical study was performed to verify the improved method. The calculation results using the improved method were compared to that of cloud method in terms of the determination coefficient, Kernel Density Estimation curve, the rank-correlation coefficient and the fragility curves. Several remarkable conclusions are drawn as follows:

(1) The structural fragility curves calculated using the cloud method may lead to errors when the PSDM shows heteroscedasticity, and the errors increase with the increasing damage degree.

(2) The improved fragility analysis method is practical, which establishes PSDM using BOX-COX regression and calculates fragility curves with the assistance of Monte Carlo Sampling technique. The PSDM established by using BOX-COX regression does not need to meet the assumptions adopted in the cloud method.

(3) When the cloud method satisfies all three assumptions, identical fragility curves are obtained using both methods.

ACKNOWLEDGMENT

This research was supported by the National Natural Science Foundation of China under Grant No. 51978511.

REFERENCES

ANCHETA, T. D., DARRAGH, R. B., STEWART, J. P., SEYHAN, E., SILVA, W. J., CHIOU, B. S. J., WOODDELL, K. E., GRAVES, R. W., KOTTKE, A. R., BOORE, D. M., KISHIDA, T. & DONAHUE, J. L. 2014. NGA-West2 Database. *Earthquake Spectra*, 30**,** 989-1005.

AVIRAM, A., MACKIE, K. R. & STOJADINOVIC, B. 2008. Effect of abutment modeling on the seismic response of bridge structures. *Earthquake Engineering and Engineering Vibration*, 7**,** 395-402.

BAKER, J. W. 2007. Probabilistic structural response assessment using vector-valued intensity measures. *Earthquake Engineering & Structural Dynamics*, 36**,** 1861-1883.

BAKER, J. W. & LEE, C. 2018. An improved algorithm for selecting ground motions to match a conditional spectrum. *Journal of Earthquake Engineering*, 22**,** 708-723.

BOORE, D. M., STEWART, J. P., SEYHAN, E. & ATKINSON, G. M. 2013. NGA-West2 equations for predicting PGA, PGV, and 5% damped PSA for shallow crustal earthquakes. *Earthquake Spectra*, 30**,** 1057-1085.

BOX, G. E. P. & COX, D. R. 1964. An analysis of transformations. *Journal of the Royal Statistical Society: Series B (Methodological)*, 26**,** 211-243.

COLLINS, S. 1991. Prediction techniques for Box–Cox regression models. *Journal of Business & Economic Statistics*, 9**,** 267-277.

CORNELL, C. A., JALAYER, F., HAMBURGER RONALD, O. & FOUTCH DOUGLAS, A. 2002. Probabilistic basis for 2000 SAC federal emergency management agency steel moment frame guidelines. *Journal of Structural Engineering*, 128**,** 526-533.

DU, A., PADGETT, J. E. & SHAFIEEZADEH, A. 2019. A posteriori optimal intensity measures for probabilistic seismic demand modeling. *Bulletin of Earthquake Engineering*, 17**,** 681-706.

FENG, R., WANG, X., YUAN, W. & YU, J. 2018. Impact of seismic excitation direction on the fragility analysis of horizontally curved concrete bridges. *Bulletin of Earthquake Engineering*, 16**,** 4705-4733.

GARDONI, P., DER KIUREGHIAN, A. & MOSALAM KHALID, M. 2002. Probabilistic Capacity Models and Fragility Estimates for Reinforced Concrete Columns based on Experimental Observations. *Journal of Engineering Mechanics*, 128**,** 1024-1038.

HUANG, Q., GARDONI, P. & HURLEBAUS, S. 2010. Probabilistic Seismic Demand Models and Fragility Estimates for Reinforced Concrete Highway Bridges with One Single-Column Bent. *Journal of Engineering Mechanics*, 136**,** 1340-1353.

HWANG, H., LIU, J. B. & CHIU, Y. H. 2001. Seismic fragility analysis of highway bridges. Urbana: Mid-America Earthquake Center.

JEON, J.-S., SHAFIEEZADEH, A., LEE, D. H., CHOI, E. & DESROCHES, R. 2015. Damage assessment of older highway bridges subjected to three-dimensional ground motions: Characterization of shear–axial force interaction on seismic fragilities. *Engineering Structures*, 87**,** 47-57.

KARAMLOU, A. & BOCCHINI, P. Quantification of the approximations introduced by assumptions made on marginal distributions of the demand for highway bridge fragility analysis. Second International Conference on Vulnerability and Risk Analysis and Management (ICVRAM 2014), 2014 Liverpool. 13-16.

MACKIE, K. & STOJADINOVIC, B. Relation between probabilistic seismic demand analysis and incremental dynamic analysis. 7th US National Conference on Earthquake Engineering, 2002 Boston. 21-25.

MACKIE, K. R. & STOJADINOVIĆ, B. 2005. Fragility basis for California highway overpass bridge seismic decision making. Berkeley: Pacific Earthquake Engineering Research Center.

MUNTASIR BILLAH, A. H. M. & SHAHRIA ALAM, M. 2015. Seismic fragility assessment of highway bridges: a state-of-the-art review. *Structure and Infrastructure Engineering*, 11**,** 804-832.

MUTHUKUMAR, S. 2003. *A contact element approach with hysteresis damping for the analysis and design of pounding in bridges.* Georgia Institute of Technology.

NIELSON, B. G. 2005. *Analytical fragility curves for highway bridges in moderate seismic zones.* Georgia Institute of Technology.

NIELSON, B. G. & DESROCHES, R. 2007a. Analytical seismic fragility curves for typical bridges in the central and southeastern United States. *Earthquake Spectra*, 23**,** 615-633.

NIELSON, B. G. & DESROCHES, R. 2007b. Seismic fragility methodology for highway bridges using a component level approach. *Earthquake Engineering & Structural Dynamics*, 36**,** 823-839.

PAN, Y., AGRAWAL, A. K. & GHOSN, M. 2007. Seismic fragility of continuous steel highway bridges in new york state. *Journal of Bridge Engineering*, 12**,** 689-699.

PARZEN, E. 1962. On estimation of a probability density function and mode. *The annals of mathematical statistics*, 33**,** 1065-1076.

PRIESTLEY, M. J. N., SEIBLE, F. & CALVI, G. M. 1996. *Seismic Design and Retrofit of Bridge*, New York, John Wiley & Sons Inc.

SCOTT, B., PARK, R. & PRIESTLEY, M. 1989. *Stress-strain behavior of concrete confined by overlapping hoops at low and high strain ratio Rates.* Doctoral Thesis, Lulea University of Technology, Lulea, Sweden.

SHAFIEEZADEH, A., RAMANATHAN, K., PADGETT, J. E. & DESROCHES, R. 2012. Fractional order intensity measures for probabilistic seismic demand modeling applied to highway bridges. *Earthquake Engineering & Structural Dynamics*, 41**,** 391-409.

SPEARMAN, C. 1904. The proof and measurement of association between two things. *American journal of Psychology*, 15**,** 72-101.

VAMVATSIKOS, D. & CORNELL, C. A. 2001. Incremental dynamic analysis. *Earthquake Engineering & Structural Dynamics*, 31**,** 491-514.

ZAR, J. H. 1972. Significance Testing of the Spearman Rank Correlation Coefficient. *Journal of the American Statistical Association*, 67**,** 578-580.

ZHONG, J., GARDONI, P., ROSOWSKY, D. & HAUKAAS, T. 2008. Probabilistic Seismic Demand Models and Fragility Estimates for Reinforced Concrete Bridges with Two-Column Bents. *Journal of Engineering Mechanics*, 134**,** 495-504.

ZHOU, L., WANG, X. & YE, A. 2019. Shake table test on transverse steel damper seismic system for long span cable-stayed bridges. *Engineering Structures*, 179**,** 106-119.